SELECTIVE ELECTROCHEMICAL REDUCTION OF CO_2 TO HIGH VALUE CHEMICALS

Grant agreement no.: 851441
***Start date**: 01.01.2020 – **Duration**: 36 months*
***Project Coordinator**: Dr. Brian Seger - DTU*

DELIVERABLE REPORT

3.1 REPORT ON CO-CATALYST APPROACH TOWARDS ETHANOL PRODUCTION	
Due Date	31/12/2020
Author (s)	Carlos Andres Giron Rodriguez, Brian Seger
Workpackage	3
Workpackage Leader	Brian Seger
Lead Beneficiary	DTU
Date released by WP leader	30/12/2020
Date released by Coordinator	30/12/2020

DISSEMINATION LEVEL		
PU	*Public*	***X***
PP	*Restricted to other programme participants (including the Commission Services)*	
RE	*Restricted to a group specified by the consortium (including the Commission Services)*	
CO	*Confidential, only for members of the consortium (including the Commission Services)*	

NATURE OF THE DELIVERABLE		
R	*Report*	***X***
P	*Prototype*	
D	*Demonstrator*	
O	*Other*	

SUMMARY	
Keywords	*Tandem electrodes, ethanol selectivity, C_{2+} products, Cu/Ag catalysts, gas diffusion electrodes, nanoparticle catalyst, spray-coating*
Abstract	Sluggish kinetics related to C-C coupling products limit the effectiveness of electrochemical CO_2 reduction to ethanol over Cu catalysts. The preparation of tandem catalysts by the deposition of two independent and adjacent layers on gas diffusion electrodes can enhance the reaction kinetics by increasing the local CO concentration. A series of Cu/Ag and Cu/Au electrodes were prepared, varying the composition through the deposition of a CO-selective layer on top of the Cu using both thin films and nanoparticles. This approach allows the Ag or Au to efficiently produce CO that can further diffuse, couple, and reduce to form ethanol and other C_2 or C_3 products. The ethanol faradaic efficiency increased from 11% to 17% at 150 mA/cm^2, when switching from a pure copper catalyst to a layered catalyst consisting of 60% Cu and 40% Ag. More broadly the faradaic efficiency of all C_{2+} products reached a maximum value of 67% with this catalyst.
Public abstract for confidential deliverables	

REVISIONS			
Version	**Date**	**Changed by**	**Comments**
0.1	26/12/2020	Carlos Andres Giron Rodriguez	

CO-CATALYST APPROACH FOR ETHANOL PRODUCTION

CONTENT

1. INTRODUCTION

Electrochemical CO_2 reduction (eCO_2R) is an alternative to mitigate greenhouse gas emissions, enabling the storage of intermittent renewable energy sources in the form of chemical feedstocks and fuels [1–3]. Despite the exhaustive investigation in discovering new catalysts for the eCO_2R, research is limited to the use of Cu as an electrocatalysts for highly reduced products since it is the only metal with negative adsorption energy for *CO and positive adsorption energy for *H. This property thus enables the reduction into alcohols and hydrocarbons [4]. Given the low Faradaic efficiency (FE) and moderate activity for C_{2+} products using only Cu, specific strategies have been established to tune the activity and selectivity into value-added chemicals, such as the formation of grain boundaries, vacancy steering, dopant modification, alloy formation with other metals to varying the position of the d-band, improvements in the surface morphology to expose the preferred crystalline facets, the manipulation of the oxidation state and the electrolyte design [5–8].

For the production of ethanol and other C_2 products on the Cu surface, the crucial step is the C-C coupling through either the *CO bonding with a hydrogenated species (*CHO) or the dimerization of adsorbed *CO. This potential for C-C coupling is limited by the possibility of the bound CO desorbing from the surface. This relationship is based on the linear scaling relation of the adsorption energy and the Brønsted–Evans–Polanyi (BEP) relationship for the activation energy with the binding energy of the key intermediate species [9–11]. Nanostructuring can enhance the electrocatalytic activity by increasing the active surface area (ECSA), the occurrence of undercoordinated sites, the readsorption of intermediate products, spillover phenomena, and faceting [6, 12–15]. The use of tandem catalysts can help also break the linear scaling reactions since the eCO_2R would happen in two different segregated actives sites, promoting the intermediates' stability adsorbate-surface interactions [4, 16-17]. While ethylene and ethanol tend to scale, it has been shown that being able to operate at lower overpotentials with enhanced CO concentrations favour oxygenated species such as ethanol over ethylene providing a potential way to selectivity increase ethanol formation [16].

Combining Cu with another CO-selective metal (Ag, Au, and Zn) should increase the CO local concentration on the Cu surface, improving the production rate and reducing the overpotentials of ethanol as well as other C_2 products [18]. In this approach CO_2 is converted first to CO, followed by dimerization and hydrogenation reactions such as ethanol on selective sites. Tandem catalysts have been reported in the literature such as core-shell Cu@Ag [18], Cu@ZnO [11], Ag-Cu nanodimers [17], and mixed Cu nanoparticles with other CO-selective catalysts (Au, Ag, ZnO, and Ni-N-C). These catalysts have exhibited higher partial current density and Faradaic efficiencies in the range of 1-4 times compared to pure Cu electrodes and alloys. Maximizing the C-C coupling depends on the metal mass loading and spatial arrangement in the catalyst layer, highlighting the importance of controlling these parameters during the synthesis process to guarantee the proper location of the active sites.

The performance of such electrocatalysts with two-sequential pathways have only been implemented in H-type cells. However, this approach has limited commercial potential due to its low current density for target products, related to the low CO_2 solubility in aqueous electrolytes and thick mass-transfer boundary layer [8]. The use of flow cells and gas diffusion electrodes (GDEs) can overcome the limitations of CO_2 mass transport and diffusion lengths within the boundary layers [19].

By using a layer-by-layer deposition approach to developing tandem catalysts (e.g. Cu-Ag) on gas diffusion layers, this simulates the operation of two simultaneous plug flow reactors (PFR) in series in one electrolyzer, where the

CO species produced on the CO-selective catalyst will later feeds into the C_{2+} selective catalyst layer (i.e. Cu) for the further reduction into the target products [11]. In addition, the fabrication and preparation of such catalysts require the sequential coating of two independent layers allows for a great deal of flexibility in tuning each layer independently thus providing an extra degree of freedom in optimizing the tandem device compared to simply mixing the catalyst together beforehand.

The following report focus on the study on tandem catalysts (Cu/Ag and Cu/Au) using a layer-by-layer electrode preparation method produced via spray-coating, with two independents layers of commercial nanoparticles. The goal was to provide high local CO concentrations around the Cu catalyst allowing these particle to maximize C-C coupling, and giving an extra parameter to modify to both improve ethanol selectivity as well as help modify the ethanol to ethylene selectivity.

2. DELIVERABLE SCOPE AND DESCRIPTION

The Deliverable 3.1 objective is to study nanoparticles-based tandem catalysts in the eCO_2R using different CO-selective catalysts (Ag and Au) over Cu to enhance the ethanol production. Given that eCO_2R produces a multitude of products, many of high value such as ethylene and CO, these results are useful not only for WP3, but also WP2 (CO Production) and WP4 (Ethylene Production). While the focus in this report is on ethanol, due to this impact on WP2, and especially WP4, we did widen the discussion to talk about all eCO_2R products, not just ethanol.

The present document reports first on general optimizations using benchmark Cu catalysts investigating whether sputtering versus spray coating is optimal for ethanol production, and the optimal current density to operate remaining tests. Since there was not a clear optimal technique for ethanol production we briefly investigated for tandem Cu:Ag catalysts, but gas products showed no signs of a synergistic effects for the tandem catalysts, so we did not continue towards the more complicated process of measuring liquid products such as ethanol. Another benchmarking approach done with pure Cu was variations in mass loadings. Again, to speed up development gas products was used as an indicator to determine the optimal loading.

Tandem catalysts were initially tested using two different approaches. The first approach was to simply mix Cu and Ag and the deposit the catalyst, with the second approach consisting of first depositing a Cu layer, and then on top of this depositing a Ag layer. In doing so this created a bit of a spatial distribution between the Ag and Cu catalysts. With the layered approach showing slightly better ethanol selectivity, we followed up this approach by varying the Cu:Ag ratio and also briefly investigating Cu:Au. In doing so we found an optimal ratio.To show reproducibility we did a second set of testing of Cu:Ag catalysts as well as tested these in the new Standardized reactor developed as part of SELECTCO2 project (Milestone 1). Both of these experiments validated the general trends seen in the first set of experiments.

SEM microscopy and XPS was used as characterization tools throughout the work and gave insight into the morphology of pre-test and post-test electrodes.

3. DISCUSSION

3.1 Experimental methods

Materials

Cu nanoparticles (25 nm) were purchased from Sigma Aldrich (99.5% purity trace metal basis), Ag nanoparticles from Fuel Cell Store (40% Ag on Vulcan XC-72, with an average particle size of 30 nm), and Au from Sigma Aldrich (20 nm, stabilized in citrate buffer). A catalyst ink suspension was prepared with Nafion (Sigma Aldrich, 5% wt.) and isopropanol (99.87, anhydrous, Sigma Aldrich). The precursor for the electrolyte solution ($KHCO_3$) came from Sigma Aldrich (99.995% trace metal basis) and was diluted in deionized water (18 MΩ) to achieve the target concentration. For the anode, commercial IrO_2-coated carbon paper electrodes (Dioxide Materials) and anion exchange membranes AEM (Sustanion membrane X37-50 RT from Dioxide Materials) were used for the electrolyzers.

Electrode preparation

Sputtered Cu, Ag, and Au were prepared by depositing 100 nm of the metal onto a gas diffusion layer at an argon pressure of 2 mTorr. The preparation of single metal nanoparticle based electrodes (Cu, Ag, and Au) was made using a spray coating (using an airbrush) technique. The catalyst ink consisted of a mixed solution of a given combination of Cu nanoparticles, Ag nanoparticles, or Au nanoparticles (20 mg of the powder) along with a Nafion ionomer solution (80 μL), and a water:isopropanol solution in 10:90 ratio, and then sonicated for 30 minutes.

For spray coating the suspension was airbrushed onto a gas diffusion layer uniformly until the desired loading was reached and then was finally dried at 105°C for 24 hours. Tandem GDEs (Cu/Ag and Cu/Au) were fabricated by sequentially spraying Cu and Ag (or Au) nanoparticles on the carbon paper using the same ink suspension method as described previously, and the loadings were controlled by the amount of catalyst coated in the gas diffusion layer (GDL).

Two types of tandem electrodes were prepared, the first type consisted of keeping the total metal loading at 1 mg/cm^2 and varying the Cu, Ag, and Au loadings from 0.1-0.9 mg/cm^2 using a layer-by-layer deposition. The other type is the deposition using a mixed solution approach. In this approach the metals are mixed together at a given ratio before deposition and the deposited as a uniform mixture all at once. In this method the total metal loading was also held at 1 mg/cm^2.

Electrode characterization

The electrode characterization was made using a scanning electron microscopy (SEM) FEI Quanta 200 FEG instrument at an accelerating voltage of 15 kV. Energy-dispersive X-ray spectroscopy (EDS) mapping of the different tandem electrodes provided information on the composition and corroborated the molar ratio. Additional characterization focusing on the catalyst surface was done with X-ray photoelectron spectroscopy (XPS), using a ThetaProbe instrument (Thermo Fisher Scientific) with monochromater Al Kα radiation (1486.7 eV) equipped with a hemispherical analyzer. The scans were made in the binding energy range of 0−1400 eV with an analyzer pass energy of 100 eV.

Electrochemical reactor set-up (Cell configuration)

The overall set-up for the electrochemical reactor testing set-up is shown in Appendix A1. The primary electrochemical reactor used was a gas diffusion electrode type reactor with a catholyte, anion exchange membrane (AEM) and IrO_2 based anode. The details of the cell can be found in Appendix A2 under the 'Teflon reactor', which is the name it will be called henceforth. For a quick screening tests of sputtered samples (Appendix A4) we used a cell described in the work by Larrazabal et al. [21]. At the end of this report we used a cell designed and built by the SELECTCO2 project henceforth denoted as the "standardized reactor" and detailed in the Deliverable D4.1. An illustration of the set-up can also be found in Appendix A2. At the beginning of this work the Standardized reactor was not sufficiently validated, thus the need for using the Teflon reactor. However, near the end the Standardized reactor was sufficiently validated that it could be used to validate the results of the Teflon reactor and allow comparisons to future work in the SELECTCO2 project.

Electrochemical tests

The electrochemical system consists of the mass flow controllers, the reactor, two electrolyte storage tanks, a pumping system, a water trap for the CO_2 off-gas, the gas chromatography (GC) system, and an ex-situ HPLC system. Depending on the cell, the flow reactor consists of a CO_2 chamber and the anolyte made from stainless steel or Teflon, and an AEM between the catholyte and anolyte chambers (Sustanion X37-50 RT). The CO_2 gas-inlet rate in the cathode was set with a defined flow rate of 20-50 mL/min depending on the experiment. The catholyte and the anolyte were fed with 1.0 M $KHCO_3$ and were recirculated continuously at an approximated rate of 50 mL/min using a diaphragm pump (Company: KNF). In the catholyte chamber, a water trap was installed on the cathodic gas outlet to avoid water droplets going into the GC. However, this did mitigate liquid vapour products (such as ethanol) from being seen in the gas chromatograph. The CO_2-electrolyzer was connected to a potentiostat as an external power source (Bio-Logic VSP 300 with booster up to 4A) to control the current densities. Standard conditions for the gas flows were defined as 273 K and 1 bar, and a Ag/AgCl was used as a reference electrode. The reactor ran galvanostatically and operated in the current density range of 50-300 mA/cm^2 at intervals of 50 mA/cm^2. The cell potential is recorded for all measurements, but is only shown for a couple of tests in this report. The geometric area for the cathode and the anode have an estimated geometric surface area for the cathode and the anode of 2.0 cm^2 for the Teflon reactor and 5.0 cm^2 for the Standardized reactor. Current interrupt measurements were made to estimate the uncompensated resistance for the Teflon reactor, while for the Standardized reactor (two electrode-cell), impedance was implemented to estimate the ohmic losses throughout the membrane.

Product distribution analysis and flow measurement

The outlet cathodic stream flow rate determined using a volumetric flow meter (MesaLabs, Defender 530+) placed upstream of the gas chromatograph (GC). The product gases were analyzed using an in-line Clarus 500/580 instrument from Perkin-Elmer, equipped with a molecular sieve 13x and Hayep Q packed columns with Ar as a carrier gas. The GC determined the gas stream's composition based on the previous calibration for each of the possible products. CO, unreacted CO_2, CH_4, C_2H_4, H_2, N_2, and O_2 were quantified using the thermal conductivity detector (TCD). Postreaction liquid products were carried out by high-performance liquid chromatography (HPLC) in an Agilent 1200 series system equipped with a Bio-Rad Aminex HPX-87H column heated to 50 °C and refractive index and diode array detectors. An aqueous solution of H_2SO_4 (5 mM with a flow of 0.6 mL/min) served as the eluent. Liquid samples were collected in the catholyte, anolyte, and CO_2-off gas compartments, but just the crossover section (Appendix 5) includes the information from the anolyte and CO_2-off gas.

3.2 Characterization

Electrode characterization

Scanning electron microscopy (SEM) results of various electrodes are presented in Figure 1. The images correspond to a blank electrode, pure metal nanoparticle catalysts (Cu and Ag) and a Cu/Ag ($Cu_{0.6}Ag_{0.4}$) tandem electrodes. All electrodes are pre-experiment.

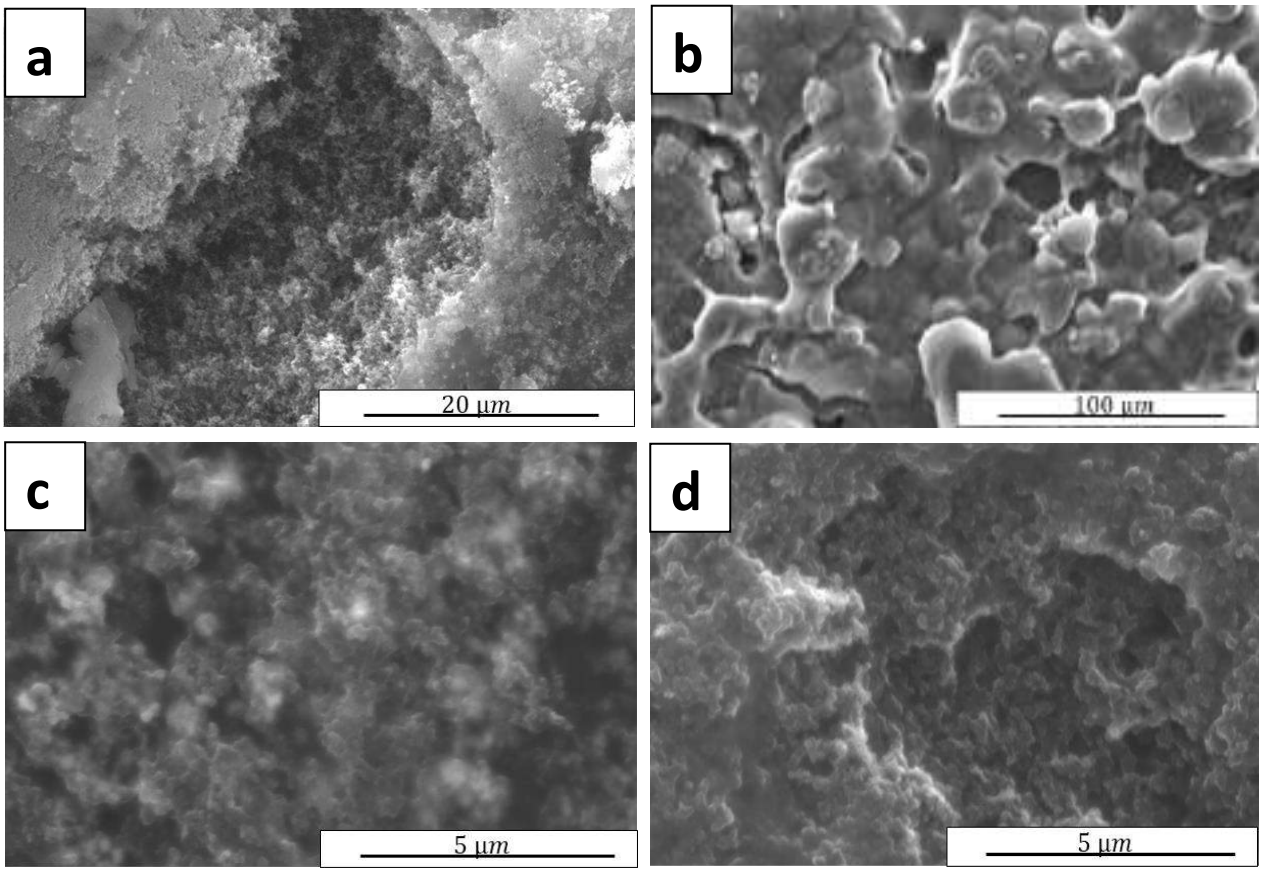

Figure 1: SEM images of gas diffusion electrodes, **(a)** Microporous carbon support **(b)** Pure Ag nanoparticles **(c)** Pure Cu nanoparticles on Sigracet 39BB **(d)** Cu/Ag tandem catalyst coated on the microporous layer

The SEM cross-section (Figure 2a) of a Cu:Ag tandem device was characterized to determine the composition of the layers allowing insight into penetration depth of the metals depending of the thickness of each layer of the GDE. The EDS elemental mapping (Figure 2b) on such samples shows the layer-by-layer structure consisting of the C, Cu, F, and Ag layers.

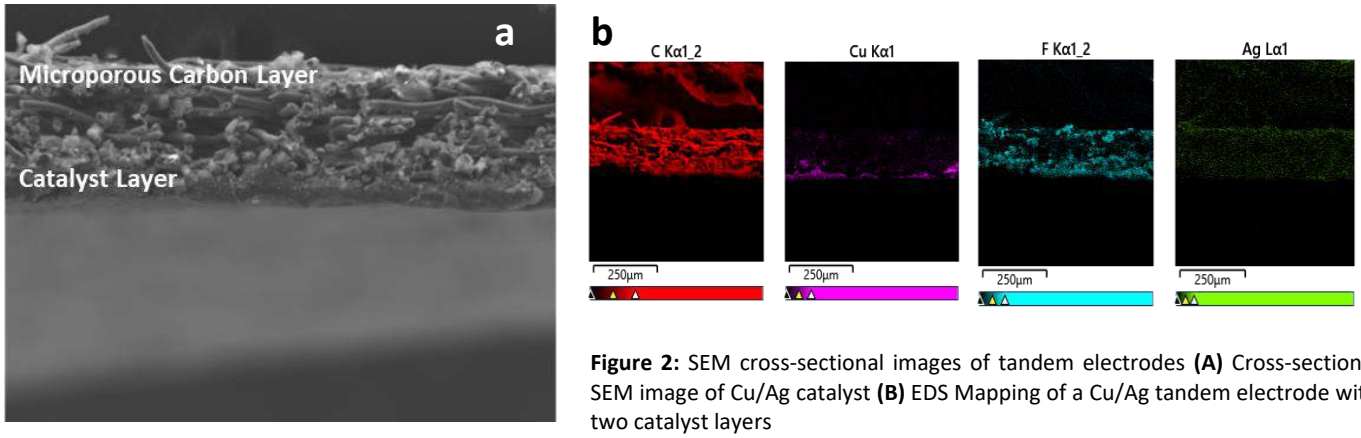

Figure 2: SEM cross-sectional images of tandem electrodes **(A)** Cross-sectional SEM image of Cu/Ag catalyst **(B)** EDS Mapping of a Cu/Ag tandem electrode with two catalyst layers

An XPS scan of the Cu-based electrodes (Figure 3) revealed the presence of copper, adventitious carbon, and oxygen and high-intensity peaks that indicate fluorine, potentially due to the Nafion layer used as a binder. Importantly no other metal impurities that might interfere with the eCO_2RR were observed within the minimum detection limit of the XPS (typically about 1%).

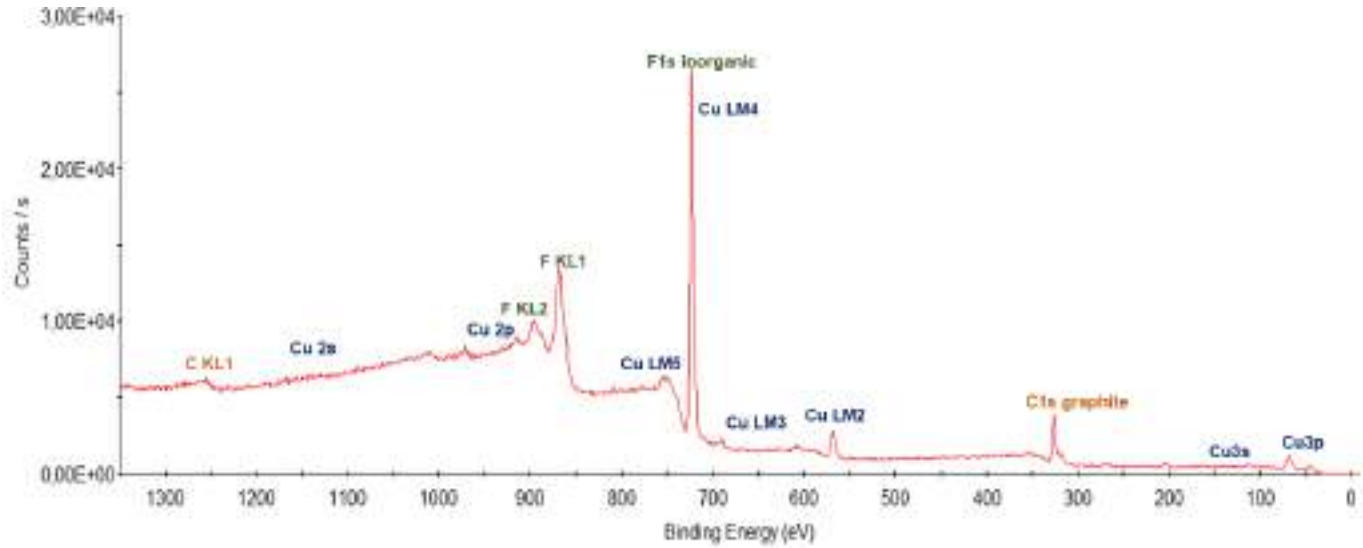

Figure 3: X-ray photoelectron spectroscopy (XPS) analysis of pure Cu nanoparticles on a gas diffusion layer electrode.

3.3 Electrode benchmark studies

Studies relating sputtering catalysts veruss spray coating catalysts.

The use of a gas diffusion electrode (GDE) facilitates CO_2 transport to the catalyst layer through the GDL, allowing optimal transport to the catholyte layer [8,19-21]. The high current density operation using a GDE can significantly reduce the local CO_2 concentration and modify the pH values in the catalyst layer [22]. The cathode layer's performance depends on the morphology and composition of the active catalyst particles, and this can be improved by enhanced exposure to the electrochemically active surface areas, and shorting of the diffusion length [19].

Common catalyst layer structures approaches in GDEs are two dimensional (2D) thin films (typically sputter deposited) and 3D nanoparticle layer (typically fabricated via dopcasting or spray coating). A 2D-film using co-sputtering deposition to fabricate different catalyst layers has been reported by Li et al. [23]., using Cu and Ag targets to produce Cu-Ag thin-films, with a Cu concentration of 70-90% producing the optimal ethanol selectivity.

As a benchmark experiment for this work, we compared a sputtered approach to a nanoparticle approach. The sputtered Cu thickness and Cu-metal loading were kept constant at 100 nm and 1 mg/cm^2, respectively. (Previous studies in terms of catalysis thickness optimization laid the basis for the method preparation and the electrode testing.[24]) Figure 4 presents the results at different current densities, using Cu nanoparticle based electrodes for both the thin films (a) and nanoparticle (b) approach.

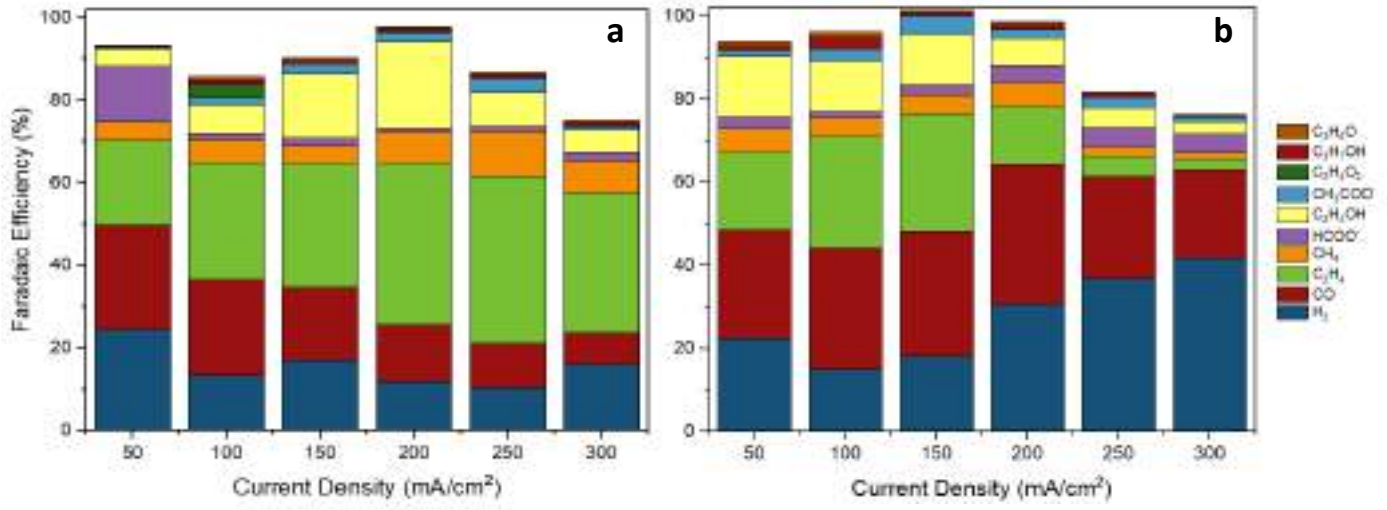

Figure 4: FE profile of Cu-based electrodes on Sigracet 39BB prepared by **(a)** Sputtering (100 nm) (**b)** by spray-coating. Experimental Conditions: CO_2 flow of 20 mL/min cm^2 in 1.0 $KHCO_3$ (catholyte and anolyte).

From Figure 4 it can be seen that both approaches can be effective at eCO_2R. Both approaches produce nearly identical H_2 selectivity's at low current densities, whereas at higher current densities the sputtered sample produces less H_2. H_2 evolution is often a sign of insufficient mass transfer of CO_2, leading to water being the only reactant, which then gets reduced to H_2. We tentatively attribute the high H_2 evolution potential in the nanoparticle system to inconsistent particle distribution entailing some particles become more easily mass transport limited with respect to CO_2. The CO selectivity is clearly higher in the nanoparticle case whereas the ethylene selectivity is higher in the sputtered case with ethanol being quite inconsistent in both cases. With CO only a partially reduced product, this does have the potential to be further reduced to ethanol, thus from that perspective the nanoparticle approach has the higher potential to selectively produce ethanol. (This is on the condition that the CO could be selectively converted to ethanol over ethylene). Additionally the nanoparticle approach is more commercially scalable and has more spatial flexibility of catalysts than a sputtered approach in which case the catalyst will always be deposited at basically the same position within a GDL.

Nevertheless, since the sputtered approach was closely comparable to the nanoparticle approach, we did a quick survey testing of the potential for co-sputtering Cu and Ag (See Appendix 4). For this quick survey we only tested gas products since this could be done much more rapidly, and it was expected there would be at least a partial scaling of ethylene with ethanol (Later in this report specifically ,Figure 8, this is clearly shown.) From these results

we did not see any synergistic effect with the co-sputtering of Cu and Ag and the electrodes acting just as Cu and Ag would independent of each other. While the Cu-Ag work appears to contradict the work of Li et al. [23], it should be noted that these tests were done on a carbon based GDL whereas the Li work was done on a Teflon based GDL so there was definitely significant fundamental differences between the two works potentially leading to the different results.

Study of the catalyst loading effect

Different Cu-nanoparticle inks' loadings were tested to achieve the optimal value following the methodology described in Section 3.1. Since the loading was measured by weighing of the GDE before and after the coating of each of the layers, this did provide a certain lack of precision, thus each loading was significantly different from the others to more broadly see the effect of loading and its impact on the catalytic performance. This also entails only a rough optimization of catalyst loading. Figure 5A shows a schematic of the ink suspension and coating on the GDE, while Figure 5B shows ethylene Faradaic efficiency for the four different samples at different current densities (the current density range was based on the results of the benchmark studies in Figure 6). Again, ethylene was used as a proxy for overall catalytic synergy effects since ethylene measurements were much quicker and this experiment and the primary purpose of this experiment was to find the general catalyst loading range that looked the most promising for eCO_2R.

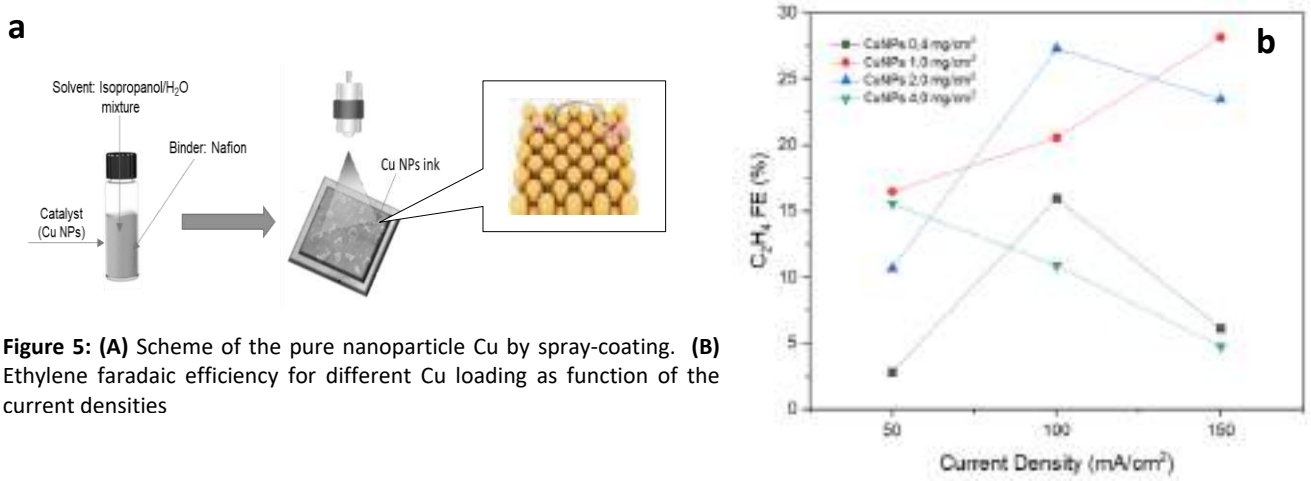

Figure 5: (A) Scheme of the pure nanoparticle Cu by spray-coating. **(B)** Ethylene faradaic efficiency for different Cu loading as function of the current densities

An optimal value for the total metal loading of the catalysis layer was found to be 1.0 mg/cm^2 based on the Faradaic efficiency of ethylene. Higher loading values generate the worst performance, which we associate to mass transfer issues, while low loadings simply have insufficient actives sites for the C_{2+} production. It should be noted that this issue was not thoroughly investigated, but just done in order to produce a near optimum loading allowing us to most clearly see trends related to varying the tandem catalyst activity.

3.4 Performance of tandem electrodes with Cu and CO-selective catalyst layers

The following section will present the results of the Cu/Ag and Cu/Au tandem catalyst in terms of layering vs. mixing, catalyst screening, and characterization.

Comparison of two-layer tandem GDE and one- mixed layer for the eCO_2R

With spray coating 1.0 mg/cm^2 of catalysts determined as the optimal conditions that should allow us to see the potential of a tandem approach most clearly, we prepared GDE's first by depositing Cu and then on top of this depositing the CO_2 to CO catalyst (either Ag or Au). Depositing the CO_2 to CO catalyst on top means that it will be closest to the electrolyte allowing produced CO to migrate to the gas diffusion electrode side to try to leave the reactor. However, on this path the CO will encounter Cu and the idea is for it to then be further reduced (hopefully to ethanol). To understand the role of the two layer approach, an alternative approach of pre-mixed Cu and Ag, were prepared, with the same metal loading as the tandem catalysts and following the same protocol described in Section 3.1. This alternative approach will act basically as a benchmark allowing us to clearly see the effect of layering. Figure 6 shows the catalyst screening results and major product distribution at different current densities for both a layered (c) and a mixture (d) of Cu:Ag nanoparticles. In these experiments the Cu:Ag ratio was 1:1 and the total metal loading was 1 mg/cm^2, thus we denote these particles as $Cu_{0.5}Ag_{0.5}$.

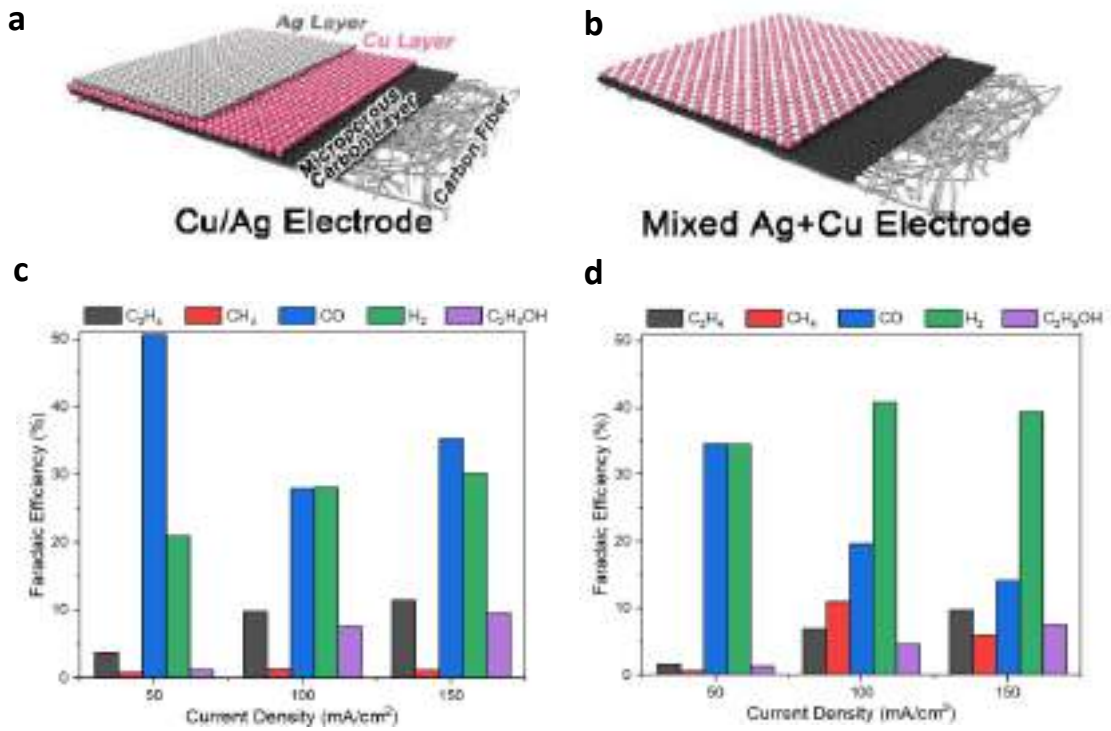

Figure 6: Schematic representation of tandem catalysts **(A)** Two-layer GDE of Cu/Ag **(B)** One-layer GDE of Cu/Ag nanoparticle mixture. FE of major products for **(C)** Tandem catalyst $Cu_{0.5}Ag_{0.5}$ and **(D)** Mixed $Cu_{0.5}Ag_{0.5}$. Images were taken from [18]. Experimental Conditions: CO_2 flow of 20 mL/min using Cu/Ag nanoparticles-based electrodes with a total loading of 1.0 mg/cm^2 on carbon paper (Sigracet 39BB) at 1.0 $KHCO_3$ (catholyte and anolyte). Tests were conducted for approximately 2 hours at the different current densities.

In comparison to pure Cu, the layer-by-layer Cu:Ag approach appeared to produce very similar product distributions of most products, which was mildly surprising since Ag is known to produce CO, and we did not see substantially more CO in this experiment. Nevertheless, the Ag could be producing CO and the Cu consuming at expected, and it could be a simple coincidence that this produced similar product selectivity. Varying the Cu-Ag ratio would help further understand this effect and is shown in the following section.

The mixed catalyst approach showed significantly higher H_2 evolution than the layer-by-layer approach. Potentially this could be due to worse catalyst dispersion in the Cu-Ag solution leading to CO_2 mass transfer issues. There is also a significant increase in methane, which is often attributed to either high overpotentials, Ni contamination or CO_2 mass transfer effects leading to H adsorption to the Cu surface, and further coupling with CO to form methane[4]. The ethanol selectivity is slightly less than the layer-by-layer approach. This may be due to the higher H_2 evolution, and thus a concomitant decrease in other products. It also could be that there is not the same local CO environment around Cu as in the layer-by-layer approach and thus a decrease in ethanol.

Catalyst screening tandem electrodes (Cu/Ag and Cu/Au) and the effect of the Cu:Ag ratio.

With the layer-by-layer approach looking slightly more promising, and having more flexibility in how we layer the different catalysts, we proceeded to investigate this further. In the following experiments we fabricated multiple Cu/Ag and Cu/Au tandem electrodes by fixing the total loading at 1.0 mg/cm^2 and varying the Cu and the Ag loadings (0.1-0.9 mg/cm^2) proportionally. These electrodes were denoted as Cu_aAg_b and Cu_aAu_b (where a and b correspond to the loading of each metal in mg/cm^2). Figure 7a shows the selectivity of a wide variety of Cu:Ag ratio catalysts operating at 150 mA/cm^2. It should be noted that since the loading are in terms of mass of the two metals, the atomic ratio will entail a significantly higher Cu percentage since it has a lower molecular weight. In addition to the Cu:Ag catalysts, we also show in Figure 7a pure Ag and Cu catalysts (both spray coated and sputtered) and a 1:1 ratio of Cu:Au catalyst. We briefly investigated Cu:Au, but since Au is significantly more expensive than Ag, these experiments did not show enough promise for us to proceed further down this more costly route.

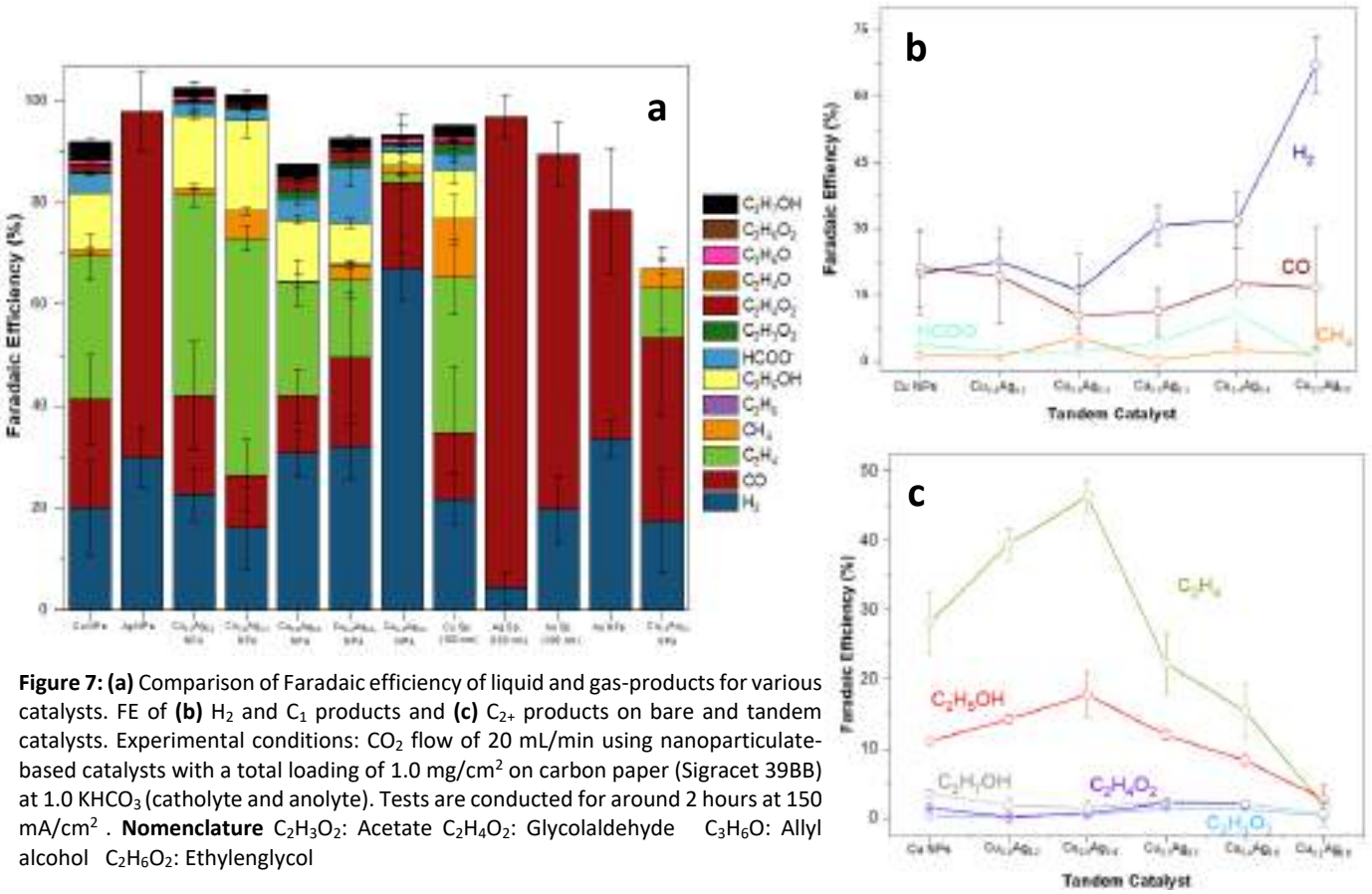

Figure 7: (a) Comparison of Faradaic efficiency of liquid and gas-products for various catalysts. FE of **(b)** H_2 and C_1 products and **(c)** C_{2+} products on bare and tandem catalysts. Experimental conditions: CO_2 flow of 20 mL/min using nanoparticulate-based catalysts with a total loading of 1.0 mg/cm^2 on carbon paper (Sigracet 39BB) at 1.0 $KHCO_3$ (catholyte and anolyte). Tests are conducted for around 2 hours at 150 mA/cm^2 . **Nomenclature** $C_2H_3O_2$: Acetate $C_2H_4O_2$: Glycolaldehyde C_3H_6O: Allyl alcohol $C_2H_6O_2$: Ethylenglycol

While Figure 7a is useful for seeing all the selectivities together for the Cu-Ag ratios, Figure 7b breaks the selectivity down into C_1 and H_2 products whereas Figure 7c breaks down the selectivity of C_{2+} products. It should be noted that in all 3 of these figures the error bars refers to multiple tests on the same electrode. From these two graphs it becomes clear that there is a peak selectivity in ethanol (as well as ethylene) at a Cu:Ag ratio of 6:4. While the atomic ratio favors Cu even more than Ag, Ag is well known to be a more efficient CO_2 to CO catalyst (which is why it is being used), thus the Ag's activity will be much higher at a given overpotential than Cu. Given current increases exponentially with overpotential (via the Tafel equation), it is quite reasonable that only a small amount of Ag is needed to balance out the copper for an optimal tandem device, as is seen in Figure 7c.

The maximum FE of C_{2+} of 67% was obtained with $Cu_{0.6}Ag_{0.4}$ at a current density of 150 mA/cm^2, however the ethanol selectivity was only 17%. Decreasing the Ag-loading below 40% starts to lead to an insufficient CO supply, which reduces the effectiveness of the Cu (since it may need to do the more inefficient CO_2 reduction instead of CO reduction) and thus decreases the C_{2+} selectivity. Additionally, the H_2 selectivity on $Cu_{0.4}Ag_{0.6}$ and $Cu_{0.2}Ag_{0.8}$ starts to increase as well. This potentially could be explained by ineffective use of the surface area on these structures and its location far from the interface. In other words, the Ag may be too deep into the electrolyte thus limiting CO_2 mass transfer to it, and favoring H_2 evolution. Additionally there could be an undetectable contamination from the Ag that is causing trouble or the small amount of copper is producing just enough liquid products to distort surface tension and create flooding. Thus, it is not clear why Ag with only a small amount of Cu produces significantly more H_2 than pure Ag nanoparticles. Nevertheless optimum values obtained in this study agree with those reported by Shen et al., where they observed the same tendency on the variation of the CO-selective layers in FE_{C2+} [18].

A further detailed breakdown of both the ethanol and ethylene selectivity's as well as their partial current density is shown in Figure 8. While the trends are clear and the total partial current density of ethanol+ethylene is approximately 100 mA/cm^2 at the optimal ratio, a careful analysis of these two graphs demonstrate that the ethanol/ethylene ratio actually gets worse at the optimal performance. Thus this approach has its advantages and disadvantages for producing ethanol.

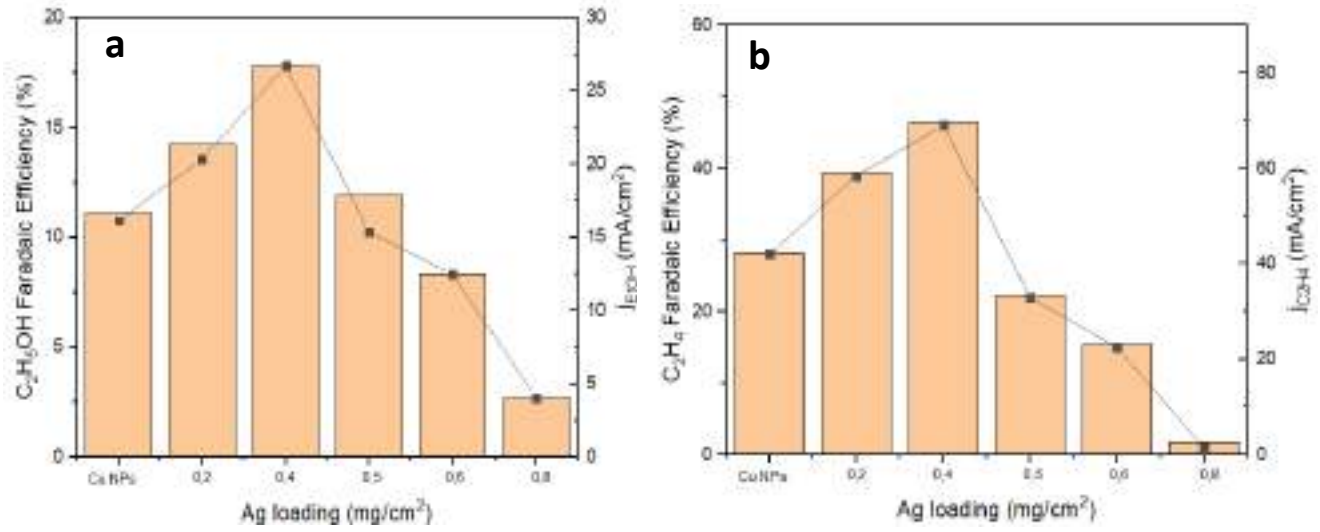

Figure 8: Comparison of the FE efficiency and the partial current density of **(a)** ethanol and **(b)** ethylene as a function of the Ag-loading.

While this approach has yet to be able to help improve the ethanol to ethylene ratio, one quite useful result is when the ethanol ratio is compared to the propanol ratio. Figure 7 shows that at the optimal Cu:Ag ratio, the ethanol

increases whereas the propanol decreases. Having an approach that selectively produces ethanol over propanol will be quite useful in obtaining our goals related to isolated ethanol selectivity for this work package in SELECTCO2.

Microscopy before and after testing optimal electrodes.

Figure 9 shows variations of the morphology of the electrodes pre-and post-experiment. While large aggregates of nanoparticles are visible on the microporous layer pre-testing, thin needle like strctures are found in the samples post-reactions. This is clearly an area of interest, and continued research will focus on why this is occurring and its influence on selectivity.

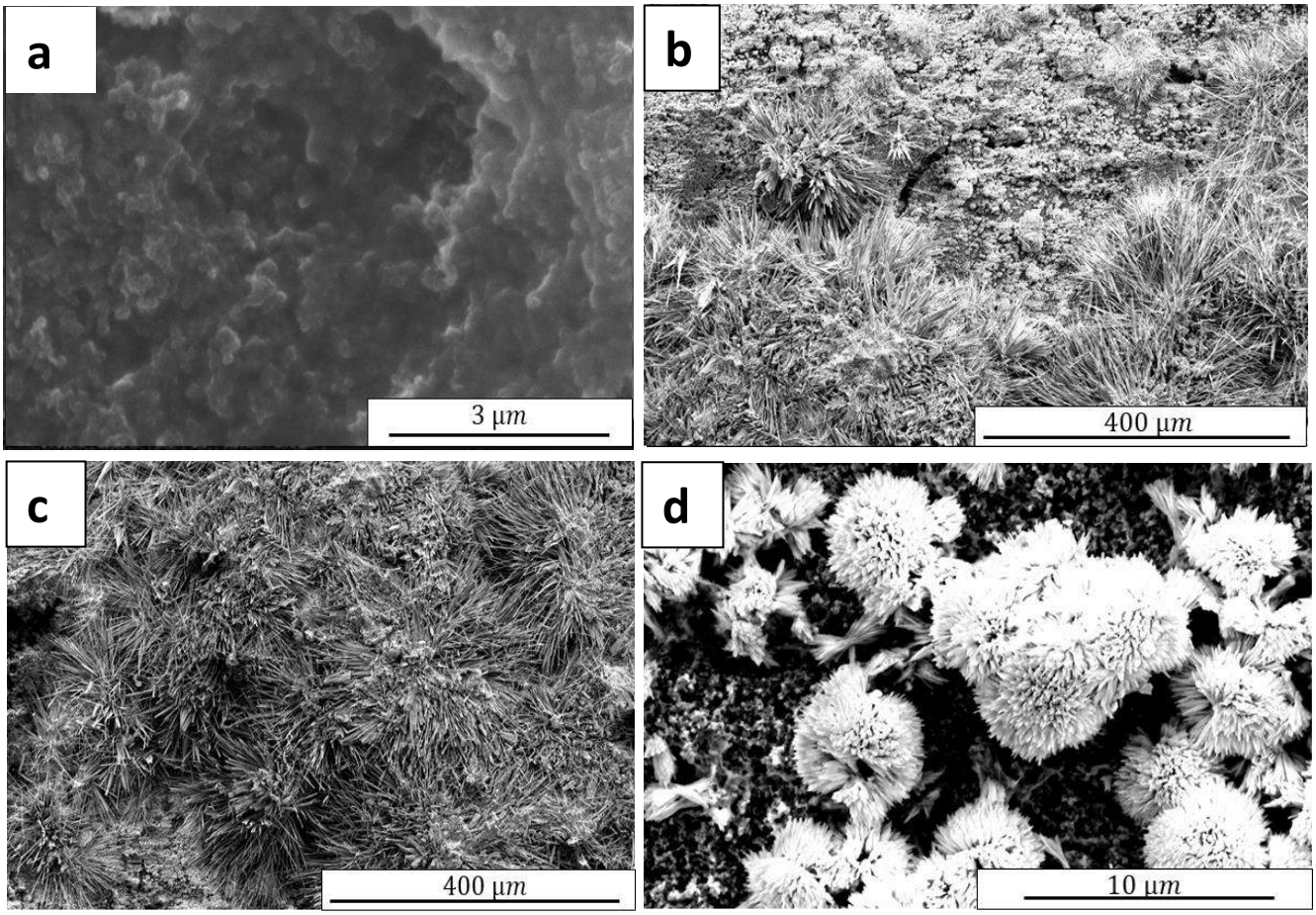

Figure 9: SEM images of the catalyst surface for the tandem Cu/Ag catalysts ($Cu_{0.6}Ag_{0.4}$) (A) Pre-experiment (B-D) Post experiments at different magnification ranges

3.5 Reproducibility

Reproducibility with the Teflon reactor

While the error bars in Figure 7 correspond to errors within a single test, we also tried completely new electrodes for all Cu, Ag, and Cu-Ag samples and these are shown in Figure 10. The experiments done in Figure 10 uses the exact same synthesis procedures and operating conditions in Figure 7 and thus represent the reproducibility of these electrodes. Given the large numbers of variables and parameters related to these experiments, the faradaic efficiency trends are quite similar for the major products. The maximum value of FE_{C2+} was found to be 64% with the $Cu_{0.6}Ag_{0.4}$ electrode similar to the results previously obtained in Figure 7. The same phenomenon at high loading

of Ag in the GDE is also observed compared to the previous experiments showing the reproducibility of this trend as well.

One notable difference is in the methane selectivity for pure sputtered Cu. During testing there were issues with Ni contamination in the sputter chamber and potentially this could have been the cause of an enhanced methane production between the experiments in Figure 7 and in Figure 10.

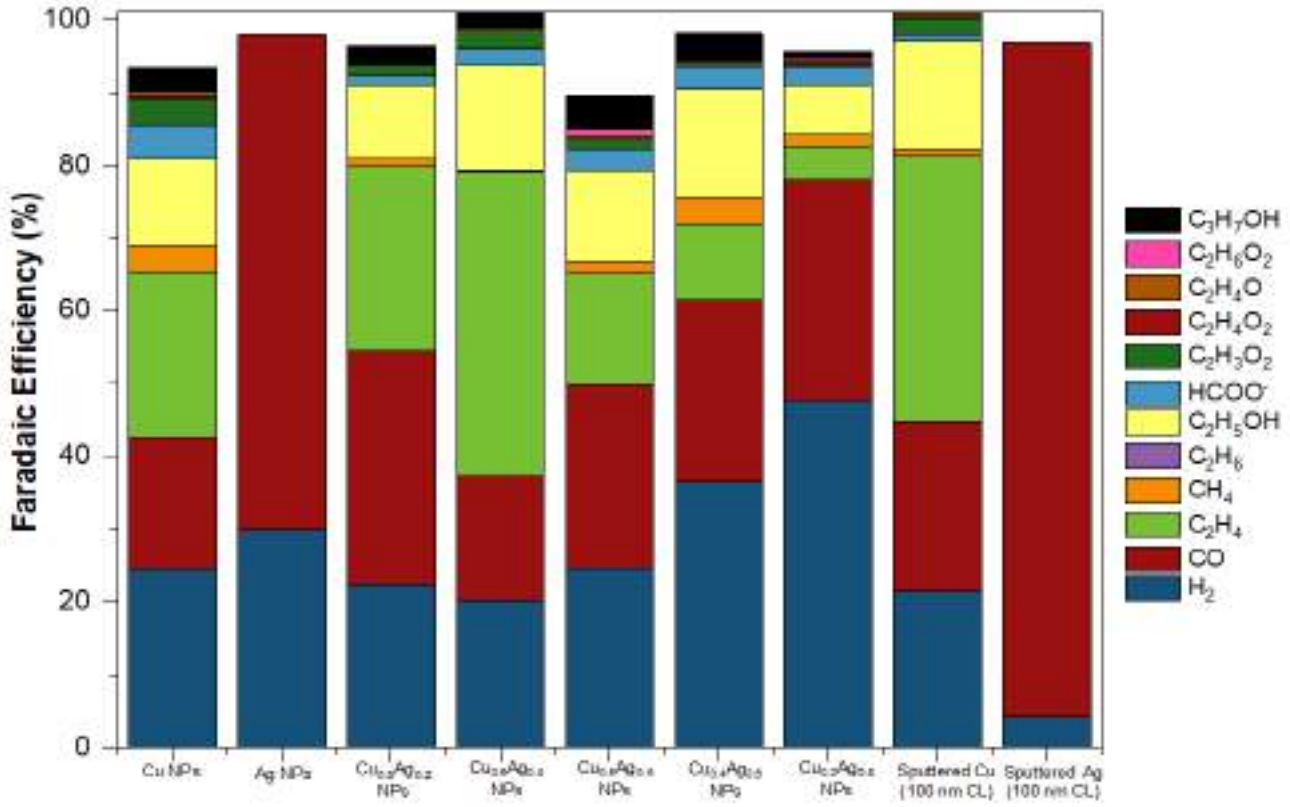

Figure 10: Comparison of Faradaic efficiency of gas and liquid-products for various electrodes. Experimental synthesis and operating parameters were the same as in Figure 7, thus this is a figure meant to show reproducibility. **Nomenclature** $C_2H_3O_2$: Acetate $C_2H_4O_2$: Glycolaldehyde C_3H_6O: Allyl alcohol $C_2H_6O_2$: Ethylene glycol

Reproducibility with the Standardized reactor

The previous experiments with the Teflon reactor featured a thick electrolyte layer between the anode and the cathode due to practicalities in the reactor design. This thick electrolyte layer introduces high ohmic resistances, causing a massive energy efficiency loss resulting in devices operating near 8 V (see Appendix 3). The Standardized reactor developed by TUD through Milestone 1 (and discussed in Deliverable 1.4) presents a thinner chamber in the case of using the catholyte thus significantly dropping the operating voltage (See Appendix A3). This reactor can also be used in a zero-gap membrane electrode assembly (MEA) approach to decrease the operating voltage even more, however this approach does not have a catholyte and thus can not remove liquid product from the reactor. Since we are not at the stage to be operating at elevated temperatures, we could not remove ethanol from the reactor via the vapor phase, thus any ethanol produced would be oxidized at the anode. For this reason we did not investigate using the tandem catalysts in the zero-gap cell.

To analyze how electrodes performed in the Standardized reactor with a catholyte, we first did a benchmark test with pure copper at various current densities as shown in In Figure 11a. The trends in this figure are as expected.

Initially we get a large amount of CO, this is followed by ethylene and ethanol with ethanol peaking first followed by ethylene. At higher current densities mass transfer issues start to dominate and H_2 faradaic efficiency grows. If we compare the 150 mA/cm^2 selectivity with the equivalent selectivity for the Teflon reactor in either Figure 7 or Figure 10, the selectivities are quite similar.

In Figure 11b we tested a smaller sample of the Cu:Ag tandem catalysts. Using the Standardized reactor these catalysts showed the same tendency for ethanol and other C_{2+} products as a function of the Ag-loading, where the sample $Cu_{0.8}Ag_{0.2}$ exhibited a maximum FE_{EtOH}=16% at 150 mA/cm^2. This value is similar to the value obtained for the optimal catalyst ($Cu_{0.6}Ag_{0.4}$) in the Teflon reactor. With the Teflon reactor having an optimal Cu:Ag ratio of 6:4 and the Standardized Reactor having an optimal ratio of 8:2, this difference can most probably be rationalized by slight experimental imprecisions or variations in reactor design. It should be noted that these experiments also show higher hydrogen production because of the electrode's carbonate formation and flooding, which seems to be more visible in the Standardized reactor due to carbonate salt precipitated in the multiple-channel serpentine flow fields. The hydroxide ions formed increased the local pH between the electrode-membrane interface, leading to carbonate formation. The GDE flooding (i.e. the carbon in the GDE becoming wetted by the electrolyte) and the liquid permeation through the microporous layer increases the diffusion length for CO_2 to the active sites, reducing the required CO_2 flow to make the CO production.

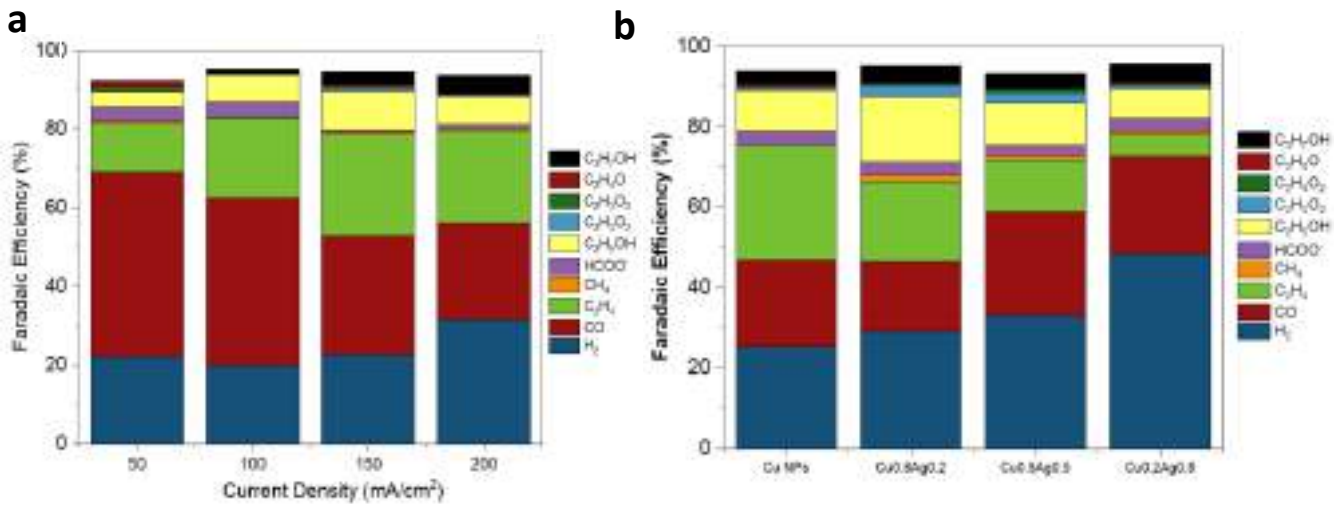

Figure 11: Faradaic efficiency of gas products using the standardized EC-reactor **(a)** pure Cu electrode **(b)** Testing of Cu/Ag tandem catalysts. Experimental conditions: CO_2 flow of 20 mL/min using Cu and Ag nanoparticle-based catalysts with a total loading of 1.0 mg/cm^2 on carbon paper-(Sigracet 39BB) in 1.0 $KHCO_3$ (catholyte and anolyte). Operational current density was 150 mA/cm^2 and test operated for approximately 2 hours. **Nomenclature** $C_2H_3O_2$: Acetate $C_2H_4O_2$: Glycolaldehyde C_3H_6O: Allyl alcohol $C_2H_6O_2$: Ethylenglycol

4. CONCLUSIONS AND FUTURE WORK

The question this report set out to answer was whether a tandem approach could be beneficial for increased selectivity to ethanol (and to a lesser extent ethylene). Unfortunately, the answer is not completely straightforward. While we did not have success co-sputtering or mixing Cu and Ag together to achieve a synergistic effect, the layer-by-layer approach did show significant promise. For our $Cu_{0.6}Ag_{0.4}$ tandem electrode we achieved a FE of C_{2+} product of 67%, which is significantly better than pure Cu nanoparticles. Furthermore, this approach increased ethanol faradaic efficiency from 11% to 17% simply by switching from a pure Cu catalyst to a $Cu_{0.6}Ag_{0.4}$ tandem catalyst. However, the ethylene faradaic efficiency improved even more with a $Cu_{0.6}Ag_{0.4}$ catalyst, thus we actually decreased

the ethanol to ethylene ratio with this catalyst. Thus while one of the original goals of this deliverable was to see if this tandem approach could favour a higher ethanol to ethylene ratio, we actually did the opposite.

As we showed throughout benchmarking, there are large number of parameters that can be modified, and simply the fact that we may be able to have an effect on the ethanol/ethylene ratio means that this approach is worth further investigations. The SEM imagery shows there is definitely a change in morphology of the catalysts over time and a better understanding of this may give much further insight into how we can modify this tandem approach to try to promote ethanol. Furthermore, consortium partner DENO is developing new gas diffusion layers and EPFL and DTU-TH are improving modelling the reaction, thus there appears to be significant potential in this approach in helping us reach the SELECTCO2 goals relating to high ethanol selectivity.

5. REFERENCES

[1] P. De Luna, C. Hahn, D. Higgins, S. A. Jaffer, T. F. Jaramillo, and E. H. Sargent, "What would it take for renewably powered electrosynthesis to displace petrochemical processes?," *Science (80-.).*, vol. 364, no. 6438, 2019, doi: 10.1126/science.aav3506.

[2] E. A. Quadrelli, G. Centi, J. L. Duplan, and S. Perathoner, "Carbon dioxide recycling: Emerging large-scale technologies with industrial potential," *ChemSusChem*, vol. 4, no. 9, pp. 1194–1215, 2011, doi: 10.1002/cssc.201100473.

[3] A. J. Hunt, E. H. K. Sin, R. Marriott, and J. H. Clark, "Generation, capture, and utilization of industrial carbon dioxide," *ChemSusChem*, vol. 3, no. 3, pp. 306–322, 2010, doi: 10.1002/cssc.200900169.

[4] S. Nitopi *et al.*, "Progress and Perspectives of Electrochemical CO2 Reduction on Copper in Aqueous Electrolyte," *Chem. Rev.*, vol. 119, no. 12, pp. 7610–7672, 2019, doi: 10.1021/acs.chemrev.8b00705.

[5] A. Ozden *et al.*, "High-rate and efficient ethylene electrosynthesis using a catalyst/promoter/transport layer," *ACS Energy Lett.*, vol. 5, no. 9, pp. 2811–2818, 2020, doi: 10.1021/acsenergylett.0c01266.

[6] R. Kas, K. Yang, D. Bohra, R. Kortlever, T. Burdyny, and W. A. Smith, "Electrochemical co2 reduction on nanostructured metal electrodes: Fact or defect?," *Chem. Sci.*, vol. 11, no. 7, pp. 1738–1749, 2020, doi: 10.1039/c9sc05375a.

[7] M. R. Singh, E. L. Clark, and A. T. Bell, "Effects of electrolyte, catalyst, and membrane composition and operating conditions on the performance of solar-driven electrochemical reduction of carbon dioxide," *Phys. Chem. Chem. Phys.*, vol. 17, no. 29, pp. 18924–18936, 2015, doi: 10.1039/c5cp03283k.

[8] S. Hernandez-Aldave and E. Andreoli, "Fundamentals of Gas Diffusion Electrodes and Electrolysers for Carbon Dioxide Utilisation: Challenges and Opportunities," *Catalysts*, vol. 10, no. 6, p. 713, 2020, doi: 10.3390/catal10060713.

[9] D. Higgins *et al.*, "Guiding Electrochemical Carbon Dioxide Reduction toward Carbonyls Using Copper Silver Thin Films with Interphase Miscibility," *ACS Energy Lett.*, vol. 3, no. 12, pp. 2947–2955, 2018, doi: 10.1021/acsenergylett.8b01736.

[10] W. Ma *et al.*, "Electrocatalytic reduction of CO2 to ethylene and ethanol through hydrogen-assisted C–C coupling over fluorine-modified copper," *Nat. Catal.*, doi: 10.1038/s41929-020-0450-0.

[11] T. Zhang, Z. Li, J. Zhang, and J. Wu, "Enhance CO2-to-C2+ products yield through spatial management of CO transport in Cu/ZnO tandem electrodes," *J. Catal.*, vol. 387, pp. 163–169, 2020, doi: 10.1016/j.jcat.2020.05.002.

[12] R. Kortlever, J. Shen, K. J. P. Schouten, F. Calle-Vallejo, and M. T. M. Koper, "Catalysts and Reaction Pathways for the Electrochemical Reduction of Carbon Dioxide," *J. Phys. Chem. Lett.*, vol. 6, no. 20, pp. 4073–4082, 2015, doi: 10.1021/acs.jpclett.5b01559.

[13] G. O. Larrazábal, A. J. Martín, and J. Pérez-Ramírez, "Building Blocks for High Performance in Electrocatalytic CO2 Reduction: Materials, Optimization Strategies, and Device Engineering," *J. Phys. Chem. Lett.*, vol. 8, no. 16, pp. 3933–3944, 2017, doi: 10.1021/acs.jpclett.7b01380.

[14] W. J. Durand, A. A. Peterson, F. Studt, F. Abild-Pedersen, and J. K. Nørskov, "Structure effects on the

energetics of the electrochemical reduction of CO2 by copper surfaces," *Surf. Sci.*, 2011, doi: 10.1016/j.susc.2011.04.028.

[15] D. Gao *et al.*, "Activity and Selectivity Control in CO2 Electroreduction to Multicarbon Products over CuOx Catalysts via Electrolyte Design," *ACS Catal.*, vol. 8, no. 11, pp. 10012–10020, 2018, doi: 10.1021/acscatal.8b02587.

[16] L. Wang *et al.*, "Electrochemical Carbon Monoxide Reduction on Polycrystalline Copper: Effects of Potential, Pressure, and pH on Selectivity toward Multicarbon and Oxygenated Products," *ACS Catal.*, vol. 8, no. 8, pp. 7445–7454, 2018, doi: 10.1021/acscatal.8b01200.

[17] J. Huang, M. Mensi, E. Oveisi, V. Mantella, and R. Buonsanti, "Structural Sensitivities in Bimetallic Catalysts for Electrochemical CO2 Reduction Revealed by Ag-Cu Nanodimers," *J. Am. Chem. Soc.*, vol. 141, no. 6, pp. 2490–2499, 2019, doi: 10.1021/jacs.8b12381.

[18] X. She, T. Zhang, Z. Li, H. Li, H. Xu, and J. Wu, "Tandem Electrodes for Carbon Dioxide Reduction into C2+ Products at Simultaneously High Production Efficiency and Rate," *Cell Reports Phys. Sci.*, vol. 1, no. 4, p. 100051, 2020, doi: 10.1016/j.xcrp.2020.100051.

[19] T. N. Nguyen and C.-T. Dinh, "Gas diffusion electrode design for electrochemical carbon dioxide reduction," *Chem. Soc. Rev.*, pp. 7488–7504, 2020, doi: 10.1039/d0cs00230e.

[20] S. Popović, M. Smiljanić, P. Jovanovič, J. Vavra, R. Buonsanti, and N. Hodnik, "Stability and degradation mechanisms of copper-based catalysts for electrochemical CO2 reduction," *Angew. Chemie Int. Ed.*, 2020, doi: 10.1002/anie.202000617.

[21] G. O. Larrazábal *et al.*, "Analysis of Mass Flows and Membrane Cross-over in CO2 Reduction at High Current Densities in an MEA-Type Electrolyzer," *ACS Appl. Mater. Interfaces*, vol. 11, no. 44, pp. 41281–41288, 2019, doi: 10.1021/acsami.9b13081.

[22] T. Burdyny and W. A. Smith, "CO2 reduction on gas-diffusion electrodes and why catalytic performance must be assessed at commercially-relevant conditions," *Energy Environ. Sci.*, vol. 12, no. 5, pp. 1442–1453, 2019, doi: 10.1039/c8ee03134g.

[23] Y. C. Li *et al.*, "Binding Site Diversity Promotes CO2 Electroreduction to Ethanol," *J. Am. Chem. Soc.*, vol. 141, no. 21, pp. 8584–8591, 2019, doi: 10.1021/jacs.9b02945.

[24] M. Ma, S. Kim, I. Chorkendorff, and B. Seger, "Role of Ion-Selective Membranes in the Carbon Balance for CO2 Electroreduction via Gas Diffusion Electrode Reactor Designs," 2020, doi: 10.26434/chemrxiv.12213215.

[25] K. Liu, W. A. Smith, and T. Burdyny, "Introductory Guide to Assembling and Operating Gas Diffusion Electrodes for Electrochemical CO 2 Reduction," *ACS Energy Lett.*, vol. 4, no. 3, pp. 639–643, 2019, doi: 10.1021/acsenergylett.9b00137.

6. APPENDIX

A1: Assembly drawings for the electrochemical cell used for the tandem electrodes

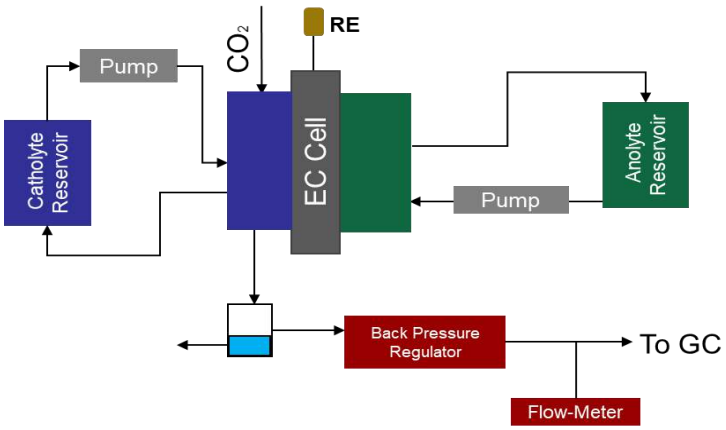

Figure A1: Flow diagram of the flow cell set-up for eCO_2R.

A2: Assembly drawings for the electrochemical cell used for the tandem electrodes

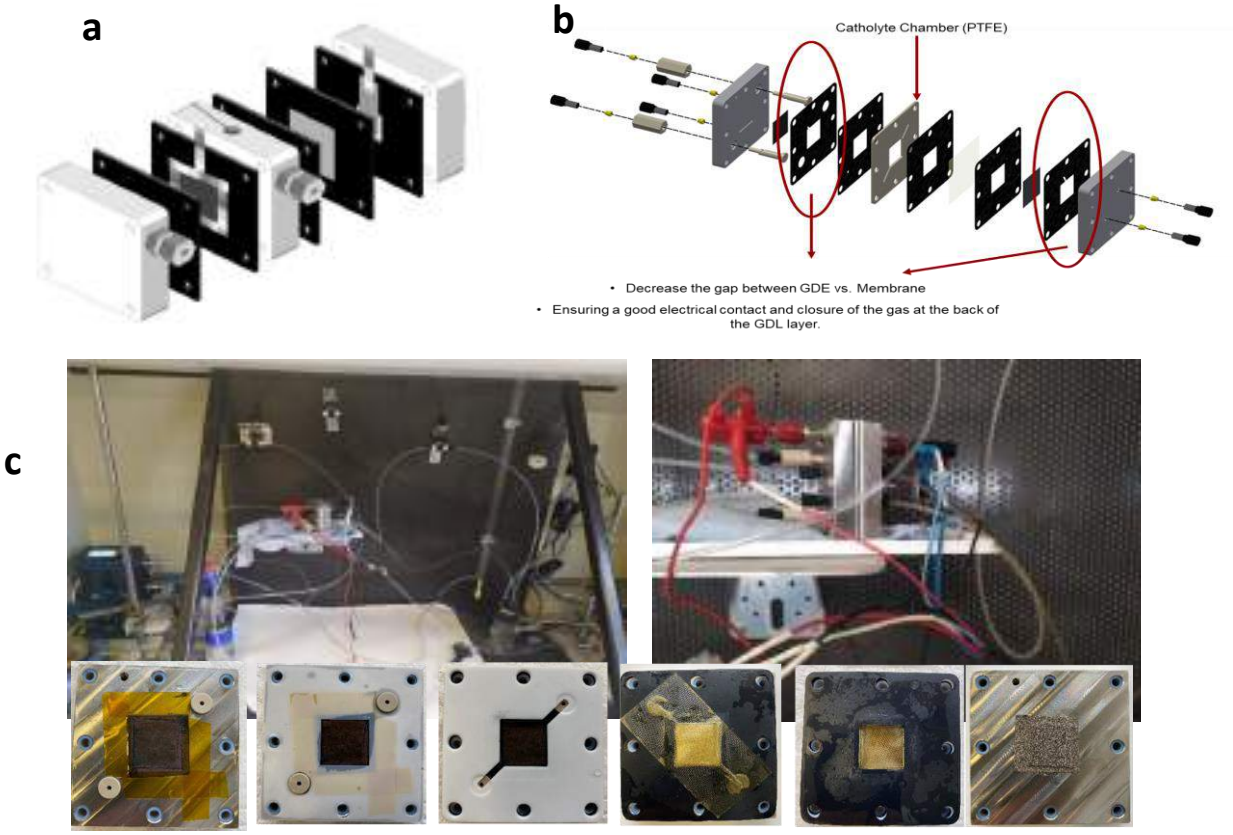

Figure A2: (a) Cartoon of the Teflon reactor, **(b)** Cartoon of the Standardized reactor and **(c)** Images of the set-up and the assembling for the Standardized reactor. Images adapted from TU Delft and Burdyny et Al. [25]

A3: Cell potential profile and electrocatalytic performance results

Results presented for the performance using the Teflon reactor (working and cell potential) for the different

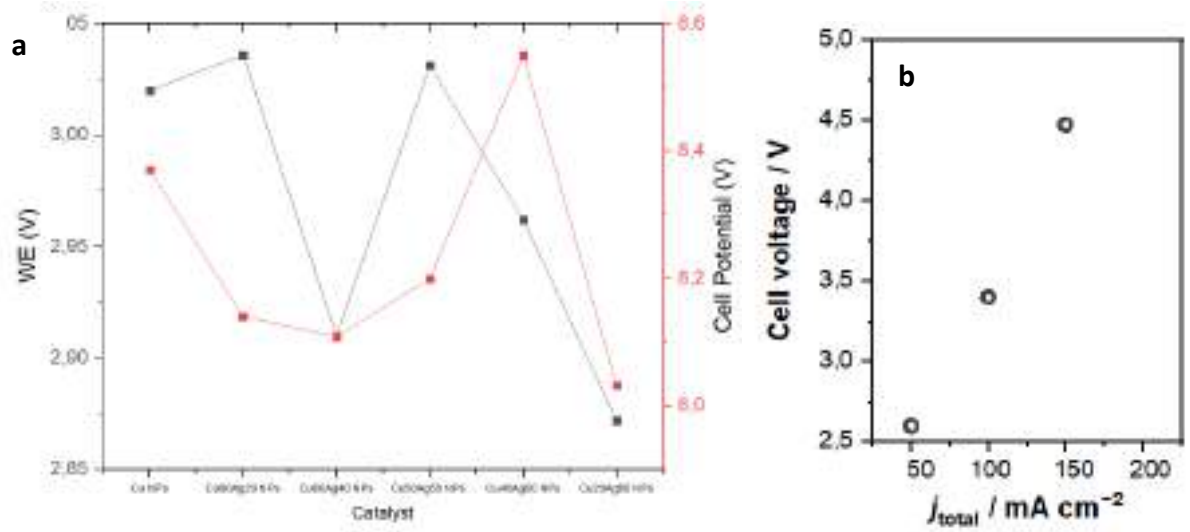

Figure A3. Electrochemical I-V data for tandem electrodes using a) the Teflon reactor @ 150 mA/cm^2 and b) the Standardized reactor with a $Cu_{0.8}Ag_{0.2}$ catalyst

A4: Cu-Ag co-catalyst approach by sputter deposition

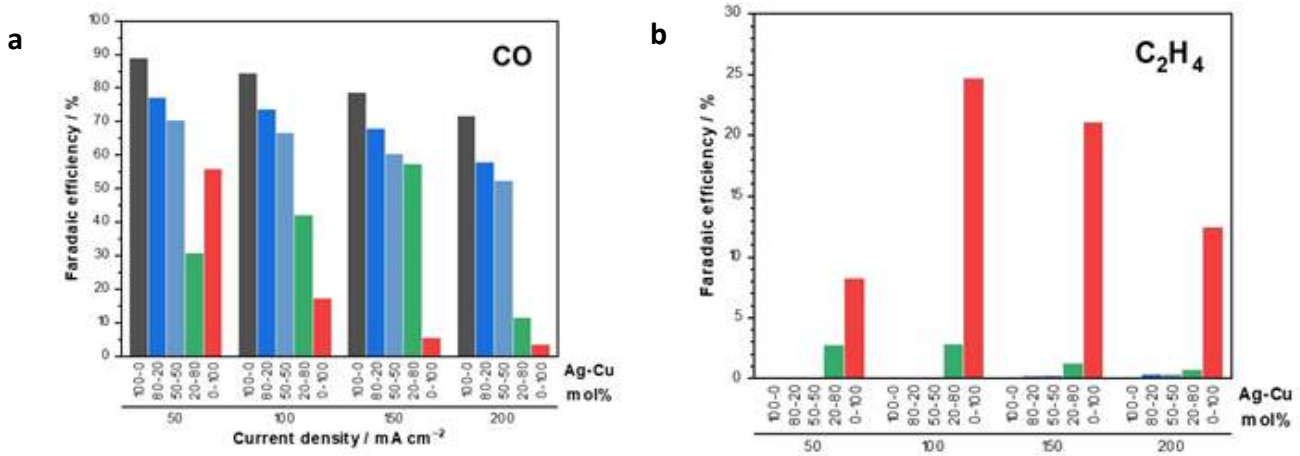

Figure A4. Faradaic efficiencies of a) CO and b) ethylene for sputtered Cu:Ag tandem catalysts